Check for updates

Chemistry–A European Journal
Research Article
doi.org/10.1002/chem.202401850
Chemistry Europe
European Chemical Societies Publishing
www.chemeurj.org

Ligand Conformation Controls Assembly of a Helicate/Mesocate, Heteroleptic $[Pd_2L_2L'_2]$ Cages and a Six-Jagged $[Pd_6L_{12}]$ Ring

Elie Benchimol,[a] Kristina E. Ebbert,[a] Alexandre Walther,[a] Julian J. Holstein,[a] and Guido H. Clever*[a]

Molecular building blocks, capable of adopting several strongly deviating conformations, are of particular interest in the development of stimuli-responsive self-assemblies. The pronounced structural flexibility of a short acridone-based bridging ligand, equipped with two monodentate isoquinoline donors, is herein exploited to assemble a surprisingly diverse series of coordination-driven Pd(II) architectures. First, it can form a highly twisted Pd_2L_4 helicate, transformable into the corresponding mesocate, controlled by temperature, counter anion and choice of solvent. Second, it also allows the formation of heteroleptic cages, either from a mix of ligands with Pd(II) cations or by cage-to-cage transformation from homoleptic assemblies. Here, the acridone-based ligand tolerates counter ligands that carry their donors either in a diverging or converging arrangement, as it can rotate its own coordination sites by 90° and structurally adapt to both situations via shape complementarity. Third, by a near 180° rotation of only one of its arms, the ligand can adopt an *S*-shape conformation and form an unprecedented C_{6h}-symmetric Pd_6L_{12} saw-toothed six-membered ring.

Introduction

Structural plasticity and adaptability are crucial characteristics of biomolecular systems. Biopolymers such as proteins, RNA, or DNA frequently undergo structural transformations to accommodate to their surroundings or modulate their activity.[1–4] Similarly, many self-assembled metallosupramolecular nanoarchitectures possess an inherent plasticity due to the dynamic nature of the constituting coordination bonds. As a result, such systems can be bestowed with the capacity to undergo directed structural transformations when subjected to external stimuli. Among the variety of coordination-driven supramolecular assemblies, metal-organic cages have emerged as a vibrant field of research as they possess the unique ability to encapsulate guest molecules within their cavities. Additionally, they can be formed as heteroleptic multicomponent assemblies[5] and participate in dynamic transformations,[6] making them ideal candidates for the development of responsive molecular systems.[7–12]

The stimuli-responsiveness of metal-organic cages has been extensively explored with respect to (sub−)component exchange,[8] guest-triggered conversion,[7] covalent post-assembly modification,[10] and light-switchable systems.[12] These studies have not only enabled access to novel structures that were not achievable through conventional self-assembly, but have also facilitated the regulation of catalytic function,[13,14] guest uptake/release,[15–20] and material properties.[21,22] Multi-stimuli-responsive systems are yet scarce and represent a challenge for the field.[23–25]

The structural flexibility of organic building blocks has always been a crucial parameter in the design of metal-organic assemblies.[26] In previous work, focus was usually set on rigid organic bridges between metal centers, or ones where conformational variability is rather limited. This led to a multitude of predictable architectures whose shapes resemble regular 3-dimensional bodies such as tetrahedra or octahedra. Recent research endeavors have started to explore the possibility of forming more intricate - often unprecedented - structural motifs by using highly flexible linkers. Hence, ligands able to adopt a set of strongly differing conformations were recognized to increase the topological complexity of metal-mediated self-assemblies.[27–30]

We, as well as others,[31–34] have previously investigated the rich assembly landscape of a peculiar ligand based on an acridone core, alkyne linkers and two isoquinoline donor groups. For example, in its crescent-shaped conformation, this ligand had been used to manifest the principle of shape-complementarity in *cis*-$[Pd_2L_2L'_2]$ heteroleptic coordination cages.[33] Unexpectedly, the same ligand also led to a novel *doubly-bridged figure-of-eight* architecture in which it adopts an *S*-shape under rotation of one of the two isoquinoline moieties.[31] Further worth noting is that we recently studied the strong axial helicity in $[Pd_2L_4]$ cages based on a carbazole ligand with the same isoquinoline donors and observed the emergence of an adjustable helicate/mesocate equilibrium.[35]

[a] E. Benchimol, K. E. Ebbert, A. Walther, J. J. Holstein, G. H. Clever
Department of Chemistry and Chemical Biology, TU Dortmund University, Otto-Hahn-Strasse 6, 44227 Dortmund, Germany
E-mail: guido.clever@tu-dortmund.de

Supporting information for this article is available on the WWW under https://doi.org/10.1002/chem.202401850

© 2024 The Authors. Chemistry - A European Journal published by Wiley-VCH GmbH. This is an open access article under the terms of the Creative Commons Attribution Non-Commercial NoDerivs License, which permits use and distribution in any medium, provided the original work is properly cited, the use is non-commercial and no modifications or adaptations are made.

© 2024 The Authors. Chemistry - A European Journal published by Wiley-VCH GmbH

Herein we present the ability of a contracted version of the previous ligand (**L1**), now carrying isoquinoline donors directly attached to the acridone backbone, to serve as the basis for an impressive structural variety of metallosupramolecular assemblies. On the one hand, a multiresponsive [Pd_2**L1**$_4$] helicate to mesocate transformation was established. Moreover, a previously unreported [Pd_6**L1**$_{12}$] six-jagged (saw-toothed) ring motif was isolated in the solid state. Finally, two *cis*-[Pd_2**L1**$_2$**L′**$_2$] heteroleptic coordination cages, carrying the acridone core with isoquinoline donors twisted by 90°, were obtained in which ligand **L1** shows its propensity to pair both with counterparts with diverging as well as converging donors. Thus, ligand **L1** gives rise to a surprisingly broad variety of self-assembled structures, simply by offering to coordinate in three distinct conformations, stemming from the slightly hindered rotation of its donor groups (Figure 1).

Results and Discussion

The structural flexibility of ligand **L1** allows the emergence of several distinct assembly motifs both in solution and the solid state. Acridone-based ligand **L1** carries isoquinoline donor groups, directly attached to the backbone via a one-step Suzuki cross-coupling reaction starting from 2,7-diiodoacridone and isoquinolin-8-ylboronic acid.

We first studied the self-assembly towards homoleptic species by combining **L1** with [$Pd(MeCN)_4$](BF_4)$_2$ in a 2:1 ratio in DMSO-d_6 and heating at 70 °C overnight. In agreement with our previously reported studies about acridone and carbazole-based palladium cages,[33,35] we observed the formation of a highly twisted [Pd_2**L1**$_4$]$^{4+}$ helicate (**H**) in which ligands are wrapped tightly around the Pd–Pd axis (Figure 2). This was first indicated by a significant upfield shift of several proton signals of **L1** (Figure 2b), indicating the influence of shielding π-planes of closely associated neighboring ligand backbones.[33,35] The formation of **H** was further supported by mass spectrometry and ^{1}H DOSY NMR (see Supporting Information, SI). Finally, crystals suitable for single X-ray diffraction analysis were obtained by slow vapor diffusion of diethyl ether into a DMSO solution of **H**, revealing the expected helicate structure (Figure 2c, left). Due to packing effects, the helicate deviates from the expected C_4 symmetry in the solid state, but the number of signals in the ^{1}H NMR spectrum undoubtedly confirms high symmetry in solution. It is interesting to note that the highly twisted character of **H** results in a rather short Pd···Pd distance of 10.25 Å, thus only leaving a small void within the assembly. The azimuthal angle defined by the pyridine-Pd vectors of a single ligand in the assembly was found to be 137° (SI).[35] In the crystal structure, one disordered chloride anion can be found in the two small pockets created between each palladium and the

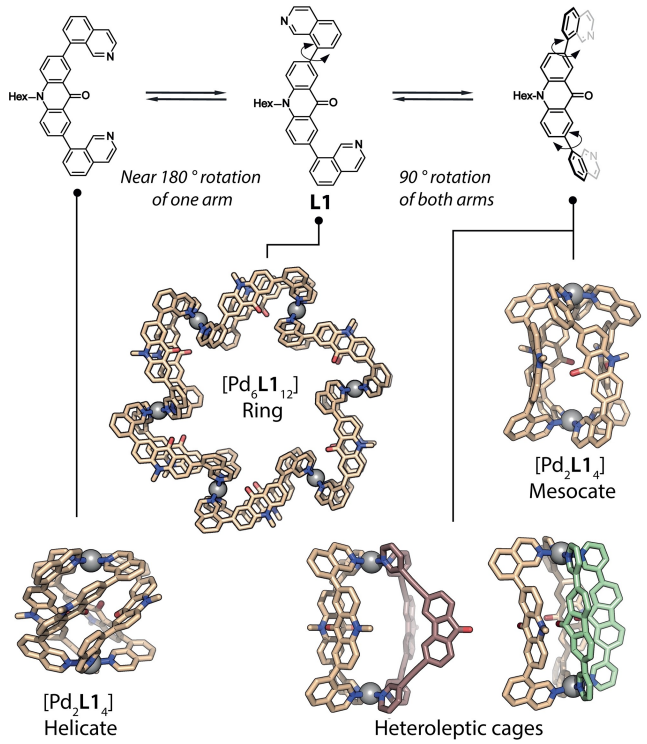

Figure 1. Ligand **L1** can adopt three different conformations resulting from the (slightly hindered) rotation of its isoquinoline donor groups around the acridone backbone. This allows the formation of a broad variety of self-assemblies, among them a [Pd_2L_4] helicate and mesocate, a [Pd_6L_{12}] ring and several heteroleptic cages.

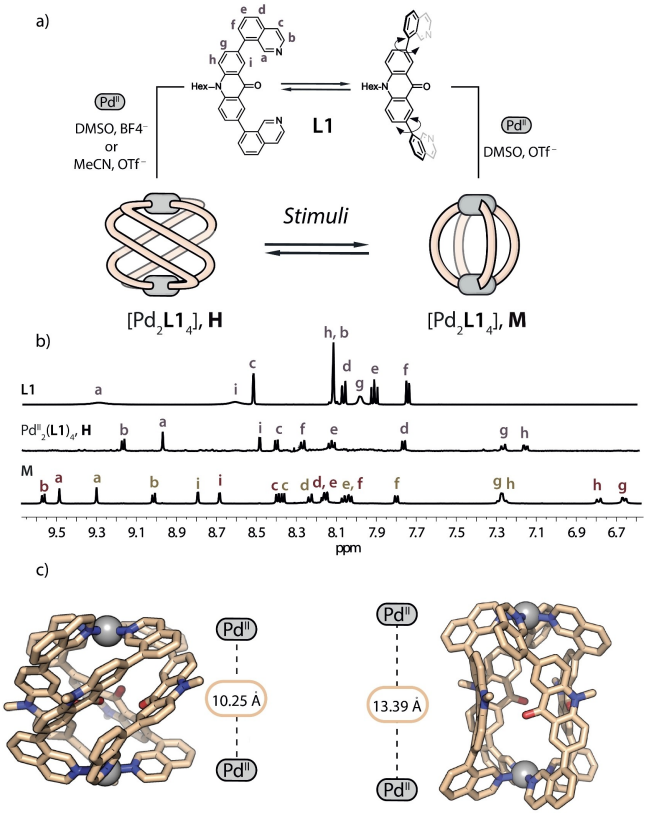

Figure 2. Transformation between helicate (**H**) and mesocate (**M**), depending on the assembly conditions. a) Schematic representation and conditions for the respective formation of **H** or **M**. b) ^{1}H NMR stack of **L1**, **H**, and **M** (500 MHz, 298 K, DMSO-d_6). c) (left) X-ray structure of **H** and (right) DFT-model (ωB97X–D/def2-SVP) of **M** (hexyl chains truncated).

© 2024 The Authors. Chemistry - A European Journal published by Wiley-VCH GmbH

15213765, 2024, 46, Downloaded from https://chemistry-europe.onlinelibrary.wiley.com/doi/10.1002/chem.202401850 by Technische Universitaet Dortmund, Wiley Online Library on [28/07/2026]. See the Terms and Conditions (https://onlinelibrary.wiley.com/terms-and-conditions) on Wiley Online Library for rules of use; OA articles are governed by the applicable Creative Commons License

central four carbonyl groups, with a 50/50% occupancy in either the top or the bottom space. This chloride could stem from impurities present in solvents or glassware during the crystallization process. However, it is likely that the cavity is vacant in solution due to the much larger size of the tetrafluoroborate counter anions. This was further supported by the presence of only a single signal in the ^{19}F NMR spectrum at 148.4 ppm, corresponding to free BF_4^- anions in solution.

Surprisingly, when the self-assembly was carried out using $[Pd(MeCN)_4](OTf)_2$ as Pd(II) source in DMSO-d_6, we observed the double number of expected ^{1}H NMR signals (in a 1:1 ratio) for **L1** (Figure 2b). This could indicate that ligand **L1** is either present in two different chemical environments within the same assembly, that its upper and lower halves are desymmetrized or that we obtained two separate species in equal ratio. Meanwhile, mass spectrometric analysis indicated the sole formation of a species of $[Pd_2\mathbf{L1}_4]$ stoichiometry, with no signs for the formation of structures of a different nuclearity (SI). The ^{19}F NMR spectrum of this sample displays two distinguishable signals for triflate at −77.74 ppm and −79.62 ppm, indicating a tightly encapsulated anion. As the X-ray structure of the helicate (see below) features a cavity too small for accommodating this anion, we inferred the formation of a mesocate assembly **M** for which molecular modeling revealed that the inner void is large enough to be occupied by one triflate molecule. NOESY NMR contacts, specific to the mesocate isomer, could further confirm this hypothesis (see Figure S22 for a complete analysis). In the signal set of the mesocate, proton Hi shows a contact to proton Hh from an adjacent ligand but also to the N–CH_2 protons of the hexyl chain. This cannot occur in the case of the helicate, where the respective distances are prohibitively large. A number of crosspeaks between the two sets of signals also strengthen the hypothesis of the formation of a single, yet desymmetrized species (SI). DOSY analysis also gives us a hint as the two sets of signals belong to a single diffusion coefficient and therefore a defined hydrodynamic radius, significantly larger than the one of **H** with 11.4 Å (but not large enough to expect a nuclearity higher than 2). Despite multiple attempts, we were unsuccessful in obtaining suitable crystals of **M**, therefore DFT modeling (ωB97X–D/def2-SVP) was carried out in order to visualize its structure (Figure 2c, right). Interestingly, the **M** isomer smoothly converged to a desymmetrized structure of point group C_1 (Figure 2c). While the rotational sense of the two Pd(quinoline)$_4$ propellers is indeed of opposite sign (as expected for a mesocate), all ligand backbones are locked into an orientation that makes all their C=O groups point to a single Pd(II) center (the lower one in Figure 2c, right), hence eliminating any horizontal mirror plane as usually observed for mesocates. This ligand conformation, where the isoquinolines rotate by an angle close to 90° in a common direction from the closely packed acridone cores, seems to reside in such a deep energetic sink that rapid flipping into its mirror image conformer is not observed even at elevated temperatures. This also results in a pronounced bending of the acridone moiety as well as an increase in the Pd···Pd distance to 13.39 Å as compared to the helicate (10.25 Å). The lateral dimensions show the opposite effect: in the helicate **H** X-ray structure, as measured between the $\underline{C}H_2$ groups attached to the nitrogen atoms of oppositely sitting backbones, they measure (on average) 14.8 Å, while the model of **M** gives 11.8 Å for the separation between the same functionalities. In most literature-reported cases of similar systems, both helicate and mesocate were described to be in dynamic equilibrium, while the factors favoring formation of the one or the other species are usually not readily explainable.[36–40]

While studying the self-assembly of **M** and **H** at room temperature, we discovered that upon rapidly recording the ^{1}H NMR spectrum after mixing **L1** with $[Pd(MeCN)_4](OTf)_2$ in DMSO, without any heating, helicate **H** was exclusively formed as a kinetic intermediate state (SI). Indeed, after 1 h at room temperature (RT), the ^{1}H NMR of the mixture shows only one set of signals, similar to what was obtained with BF_4^-. The formation of **M** can therefore be followed over time as presented in Figure 3a. Upon heating at 80 °C, the helicate (kinetic state) is rapidly forming and converts into **M** (thermodynamic state) over the course of five hours.

In order to investigate the potential responsiveness of the transformation between the helicate and the mesocate, we first attempted the formation of the cages in CD_3CN. Both the use of BF_4^- or OTf^- as counter anions yielded only helicate **H**, as only one set of signals was observed in the ^{1}H NMR spectrum (SI). **H** exists as a mixture of two quickly exchanging chiral *P* and *M* conformers as confirmed by a diastereotopic splitting of the signals of the N–$C\underline{H}_2$ protons of the hexyl chains. We wondered whether a variation in temperature, solvent and anion can be employed to trigger interconversion between the **H** and **M** topologies.

Indeed, freeze-drying a solution of preformed **H** (anion = OTf^-) in CD_3CN and redissolving the obtained solid in DMSO-d_6 led to the formation of **M** after heating the solution to 70 °C for one hour (Figure 3b). However, in a similar manner to what was observed from studying the self-assembly in DMSO at RT, the conversion from redissolved **H** to **M** at RT was rather slow and happened over the course of one day (SI). Freezing a DMSO solution of trapped **H** was found to stabilize the helicate for several days (SI). Thus, the temperature can be considered a trigger to force or prevent the formation of mesocate **M**. The inverse phenomenon in CD_3CN, the full conversion of freeze-dried **M** to **H**, was observed to be much faster, taking only one hour to complete at RT, although **M** could still be observed as an intermediate species. This constitutes the only experiment in which we could transiently observe **M** in acetonitrile. This noticeable solvent impact was also highlighted by titrating DMSO-d_6 into a solution of **H** in CD_3CN (SI). To our surprise, only 1% of DMSO-d_6 was found to be sufficient to observe the emergence of **M**, with full conversion being reached after addition of 25% DMSO. Whilst a few solvent-dependent cage-to-cage transformations have been reported before, such titrations have rarely been conducted. In comparison with the aforementioned studies, here only the conformation of the assembly is affected, while its nuclearity stays the same.

Next, an anion-induced transformation was envisaged, since BF_4^- and OTf^- were already known to yield **H** and **M**,

© 2024 The Authors. Chemistry - A European Journal published by Wiley-VCH GmbH

15213765, 2024, 46, Downloaded from https://chemistry-europe.onlinelibrary.wiley.com/doi/10.1002/chem.202401850 by Technische Universitaet Dortmund, Wiley Online Library on [28/07/2026]. See the Terms and Conditions (https://onlinelibrary.wiley.com/terms-and-conditions) on Wiley Online Library for rules of use; OA articles are governed by the applicable Creative Commons License

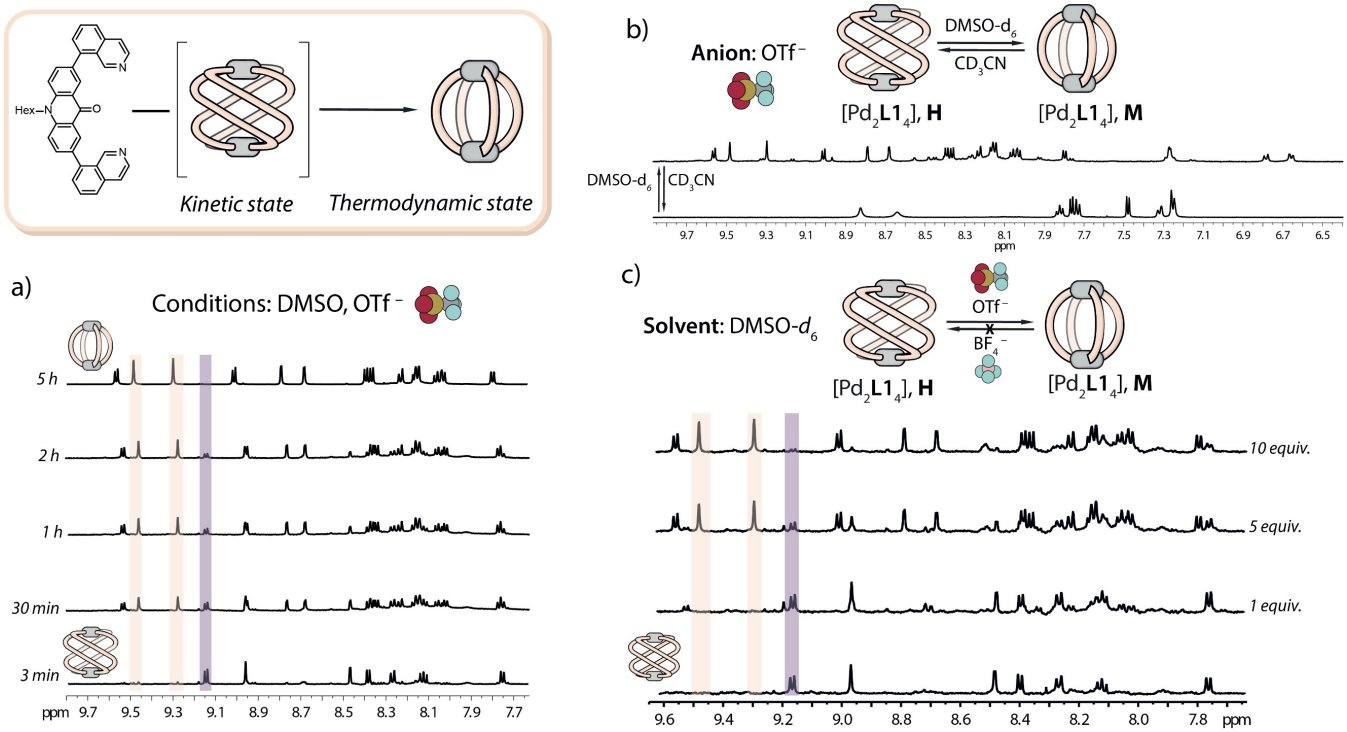

Figure 3. Stimuli-response of the **H** and **M** transformation. a) Self-assembly of **L1** with Pd(II) in the presence of triflate in DMSO leads to the kinetic formation of helicate **H**, only (purple). Heating the sample at 80 °C triggers the conversion into **M** (beige). b) Solvent switching between MeCN and DMSO allows the switch between **H** and **M**. c) **H** can be pre-formed in the presence of BF_4^- in DMSO. Introduction of triflate leads back to the **M** assembly.

respectively, in DMSO-d_6. Titration of tetrabutyl-ammonium triflate to a solution of **H** led to complete conversion into **M** after the addition of 10 equivalents (Figure 3c). In contrast, the addition of up to 10 equivalents of tetrabutyl-ammonium tetrafluoroborate into a solution of **M** was found to have no effect (SI).

Both of the previously described phenomena indicate a strong dependence of the formation of **M** on the presence of OTf^-. Indeed, as described above the ^{19}F NMR spectrum of **M** shows two distinguishable signals, highlighting the anion's role to template the formation of **M**. Moreover, neither **M** nor **H** were found to bind anionic (other than triflate) or neutral guest molecules in both CD_3CN and DMSO-d_6. This however is not surprising, considering the structures of the two different architectures, both featuring very narrow or triflate-filled cavities, respectively.

When trying to grow crystals from the different systems, we encountered another intriguing phenomenon. Slow diffusion of toluene into a DMF/DMSO solution of **H** (with BF_4^-), afforded long yellow crystalline needles suitable for crystal structure analysis by synchrotron diffraction. To our surprise, X-ray crystallographic analysis revealed a double-layered [Pd_6**L1**$_{12}$] ring with a C_{6h}-symmetric saw-toothed structure as depicted in Figure 4. To the best of our knowledge, this is the first example of a non-templated [Pd_6L_{12}] ring (with only one anion-templated 6-ring reported by Sun before[41]), while most other Pd-mediated assemblies isolated with the same nuclearity are octahedra (for another topology see[42]). Indeed, we have recently shown that there is a delicate relationship between ligand binding angles and the formation of [Pd_2L_{2n}] rings of a nuclearity larger than four.[43]

In the here found structure, the ligand adopts an *S*-shaped conformation where one isoquinoline donor rotates by nearly 180°, thus representing a third conformation for **L1**. We had previously observed this conformation for another acridone-based ligand, giving rise to a *figure-of-eight* heteroleptic cage, with two *S*-shaped ligands crossing each other in an antiparallel fashion and coordinating in a *trans*-relationship to the Pd(II) cations.[31] In the structure of [Pd_6**L1**$_{12}$], however, pairs of ligands in their *S*-shape configuration bridge neighboring palladium nodes in a parallel mode, where they end up in a *cis*-arrangement. The Pd···Pd distance of the closest palladium pair was found to be 12.87 Å, thus in-between the Pd···Pd distances determined for **H** and **M**. All carbonyl groups of the acridone cores are directed inside the ring whilst all hexyl chains point outwards, creating a rare C_{6h}-symmetric structure. In the crystal, the rings neatly stack into tubes (Figure 4), creating two types (hexagonal and triangular) channels within the porous solid (SI). The hexagonal channels go through the stacked rings and therefore their edges are defined by the 12.87 Å Pd···Pd distance given above. On the other hand, the triangular pores are demarcated by larger Pd···Pd distances of 19.67 Å and are mostly filled by the outer pointing hexyl chains of **L1**. This architecture and its packing are reminiscent of hexameric ion channels found in biological systems.[44,45] The hexagonal channels were found to be filled with disordered anions and solvent molecules.

© 2024 The Authors. Chemistry - A European Journal published by Wiley-VCH GmbH

15213765, 2024, 46, Downloaded from https://chemistry-europe.onlinelibrary.wiley.com/doi/10.1002/chem.202401850 by Technische Universitaet Dortmund, Wiley Online Library on [28/07/2026]. See the Terms and Conditions (https://onlinelibrary.wiley.com/terms-and-conditions) on Wiley Online Library for rules of use; OA articles are governed by the applicable Creative Commons License

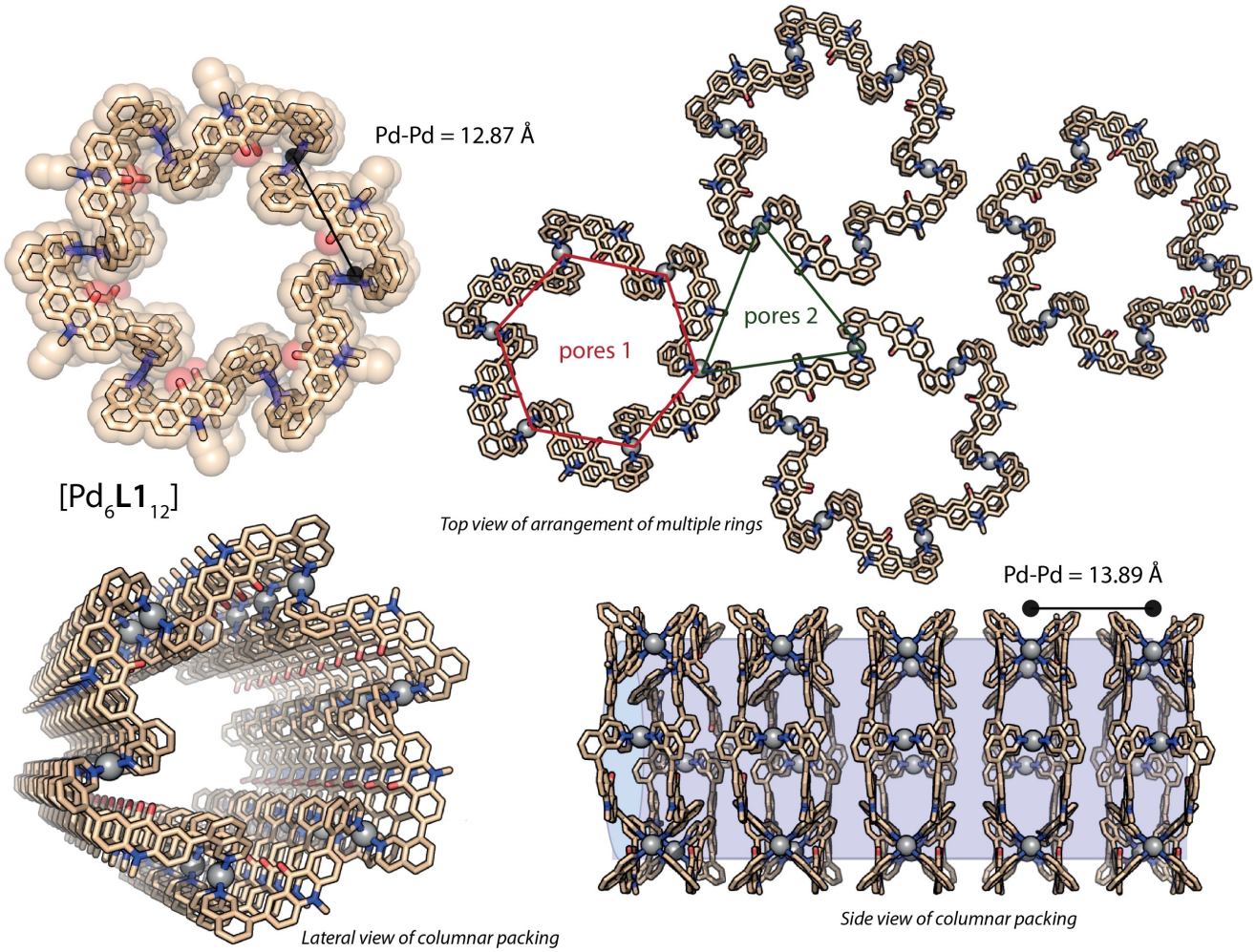

Figure 4. Crystal structure of the six-jagged $[Pd_6(\mathbf{L1})_{12}]$ ring structure. Several views of the packing are depicted to highlight the positioning of neighboring rings in the same plane and in columnar tubes orthogonal to the planes. The two types of porous channels are highlighted and key Pd···Pd distances are given.

Despite numerous attempts, however, we were never able to detect this species in solution or the gas phase, even when using cryo-ESI-MS right after dissolution of the crystals in DMSO. We therefore infer this 6-ring to exist only in the solid state and to be a crystallization-induced species, as observed previously in coordination-driven assemblies.[46,47] When dissolved, the structure collapses into the thermodynamically more favored $[Pd_2\mathbf{L1}_4]$ compound.

Eventually, we examined the capabilities of **L1** in the non-statistical assembly of heteroleptic cages (Figure 5). First, helicate **H** ($[Pd_2\mathbf{L1}_4]$; solvent = CD_3CN; anion = BF_4^-) was used to drive the transformation of a previously reported mixture of ring $[Pd_3\mathbf{L2}_6]$ and tetrahedron $[Pd_4\mathbf{L2}_8]$, obtained from fluorenone based ligand **L2**,[48] into heteroleptic cage $[Pd_2\mathbf{L1}_2\mathbf{L2}_2]$. The integratively self-sorted product could be obtained by either overnight heating of a mixture of **L1**, **L2**, and $[Pd(MeCN)_4](BF_4)_2$ in a 1:1:1 ratio at 70 °C in CD_3CN, or through cage-to-cage transformation by combining solutions of both homoleptic assemblies, containing equimolar amounts of the respective ligands. Thereby, it can be concluded that cage $[Pd_2\mathbf{L1}_2\mathbf{L2}_2]$ is the thermodynamic outcome of the reaction between these two species, induced by entropy-driven nuclearity decrease of the pre-formed $[Pd_3(\mathbf{L2})_6]$/$[Pd_4\mathbf{L2}_8]$ mixture. Mass spectrometric analysis confirmed the formation of $[Pd_2\mathbf{L1}_2\mathbf{L2}_2]$, while ^{1}H DOSY NMR allowed us to determine its hydrodynamic radius (r_h = 1.1 nm; SI), in line with previously reported values for comparable $[Pd_2A_2B_2]$-type assemblies.[6] We also tried to further increase the heteroleptic complexity of the assembly by mixing a 2:1:1 combination of **L1**, **L2** and the dimethyl fluorene analog of **L2**, **L2b** (see SI for structure) with $[Pd(MeCN)_4](BF_4)_2$ in CD_3CN. Heating the mixture at 70 °C overnight did not give a ^{1}H-NMR spectrum possible to analyze as the signals were strongly broadened. However, ESI-MS analysis yielded a series of peaks corresponding to $[Pd_2\mathbf{L1}_2\mathbf{L2L2b} + nBF_4]^{(4-n)+}$ with n = 0–2 (SI). Crystals were obtained by slow diffusion of diethyl ether into an acetonitrile solution of the ligand mixture with Pd(II). The cage crystalizes in the *Pmmn* (59) space group. The asymmetric unit contains one half of acridone ligand **L1** and one half of a superposition of **L2** and **L2b**, the final assembly being reconstructed through symmetry operations. The relative

© 2024 The Authors. Chemistry - A European Journal published by Wiley-VCH GmbH

15213765, 2024, 46, Downloaded from https://chemistry-europe.onlinelibrary.wiley.com/doi/10.1002/chem.202401850 by Technische Universitaet Dortmund, Wiley Online Library on [28/07/2026]. See the Terms and Conditions (https://onlinelibrary.wiley.com/terms-and-conditions) on Wiley Online Library for rules of use; OA articles are governed by the applicable Creative Commons License

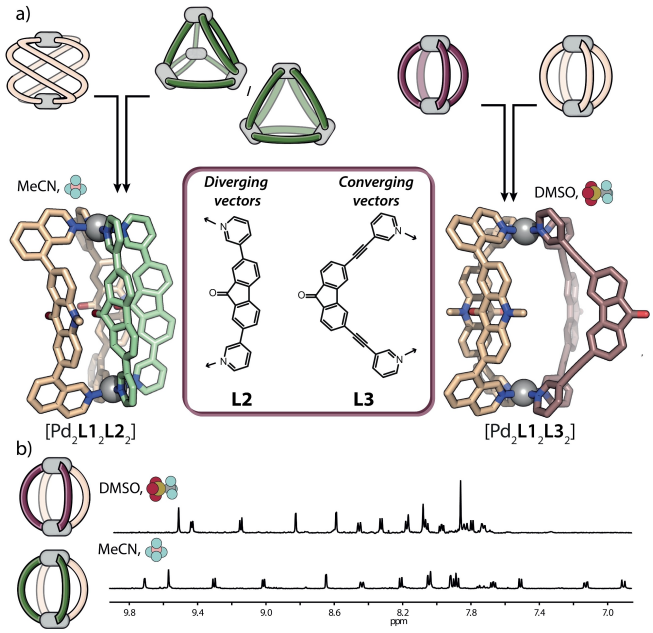

Figure 5. Use of ligand **L1** in cage-to-cage transformations to obtain heteroleptic assemblies. a) Comparison of the formed structures reveals that **L1** adapts its coordination vectors to suit both counter ligands with diverging (left) or converging (right) donor geometries. The model of $Pd_2(\mathbf{L1})_2(\mathbf{L2})_2$ based on the crystal structure data is presented on the left and the DFT model (ωB97X–D/def2-SVP) of $Pd_2(\mathbf{L1})_2(\mathbf{L3})_2$ is shown on the right. b) NMR spectra (500 MHz, 298 K, solvent indicated) of non-statistically assembled $[Pd_2\mathbf{L1}_2\mathbf{L3}_2]$ (top) and $[Pd_2\mathbf{L1}_2\mathbf{L2}_2]$ (bottom).

occupancy of **L2** was measured to be 57%, compared to 43% for **L2b**. As $[Pd_2\mathbf{L1}_2\mathbf{L2b}_2]$ was neither observed to form in solution, nor by ESI-MS in the gas phase, we assume the crystal to be composed of a majority of cis-$[Pd_2\mathbf{L1}_2\mathbf{L2L2b}]$, completed by a smaller amount of $[Pd_2\mathbf{L1}_2\mathbf{L2}_2]$, both occupying similar positions in the lattice. Owing to the close structural resemblance of **L2** and **L2b**, the two cages co-crystalize in a random manner, making it crystallographically impossible to differentiate one from the other.

In a similar fashion, a third coordination cage could be used to form another $[Pd_2A_2B_2]$-type assembly. For this purpose, we found that our previously reported cage $[Pd_2\mathbf{L3}_4]$, obtained from ligand **L3**[49] with $[Pd(MeCN)_4](OTf)_2$ in a 2:1 ratio in DMSO, was a suitable candidate. As a matter of fact, when **M** and this cage were mixed in a 1:1 ratio, we observed the emergence of a new species. Here again, all the signals belong to a single assembly with a *cis*-$[Pd_2\mathbf{L1}_2\mathbf{L3}_2]$ structure as confirmed by ^{1}H-DOSY NMR and ESI-MS (SI).

While the previously reported heteroleptic *doubly-bridged figure-of-eight* obtained from a longer acridone ligand and the *hexyl*-carbazole analog of **L3** was characterized by two sets of signals in the ^{1}H NMR spectrum,[31] owing to the unsymmetrical nature of the acridone backbone, here only one set signals was obtained. This brought us to the conclusion that no interlaced species was formed and that we obtained an assembly where **L1** possessed a similar conformation as in **M**, although herein adopting a more symmetrical arrangement. We thus created a reasonable DFT model (ωB97X–D/def2-SVP) of the *cis*-heteroleptic cage (Figure 5a, for details see the SI).

This ligand conformation, where both isoquinolines rotate by 90° in the same direction from the backbone, is the only one allowing shape complementarity between **L1** and other ligands, thus leading to a heteroleptic assembly outcome. Interestingly, **L1** is capable of associating with ligands having either diverging (**L2**) or converging (**L3**) binding vectors. In the case of $[Pd_2\mathbf{L1}_2\mathbf{L2}_2]$, the two planes defined by each of the Pd(II) centers and the nitrogens of the four corresponding donors are tilted by an angle of 13.25° for the lowest-energy conformer (SI). On the other hand, for the lowest-energy conformer of $[Pd_2\mathbf{L1}_2\mathbf{L3}_2]$ the tilting is only of 1.73° (SI).

Conclusions

In this study, we describe the formation of multiple metallosupramolecular species derived from a short acridone-based ligand with two isoquinoline donors. The conformational flexibility of this organic building block allows it to offer a variety of coordination vectors, leading to the formation of a helical cage, a mesocate, a unique Pd_6L_{12} ring in the solid-state, as well as various heteroleptic assemblies.

We have deciphered the high responsiveness of the helicate/mesocate transformation in solution, demonstrating that even subtle solvent effects and the choice of a specific anion can alter the balance between these assemblies. While the influence of the solvent is challenging to understand, the dependence on the anion can be explained by considering the cavity size. The crystal structure of the six-jagged Pd_6L_{12} ring reveals that neighboring rings assemble into supramolecular columns. In this architecture, the ligand adopts an *S*-shaped conformation, with the isoquinoline donors pointing in opposite directions. Eventually, we demonstrate that this ligand can also form heteroleptic assemblies via integrative self-sorting. The donor groups undergo a 90° rotation, and the acridone core can bend to accommodate counter ligands with both converging and diverging coordination vectors. These findings highlight the flexibility of the shape complementarity concept and encourage us to explore more ligand combinations, aimed at further enhancing structural complexity and functionality. The shown versatility of this single ligand, allowing a network of transformations between different assembly motifs, allows its incorporation into complex multi-stimuli-responsive systems with application potential as selective receptors, tunable catalysts and nanostructured materials.

Experimental Section

Synthesis of Ligand L1

2,7-Diiodoacridone **1** (500 mg, 0.94 mmol, 1 equiv.), isoquinolin-8-ylboronic acid (488 mg, 2.82 mmol, 3 equiv.) and potassium carbonate (390 mg, 2.82 mmol, 3 equiv.) were added to a 25 mL mixture of toluene, ethanol and water (4:1:1). The mixture was degassed via several freeze-pump-thaw cycles. Then

© 2024 The Authors. Chemistry - A European Journal published by Wiley-VCH GmbH

15213765, 2024, 46, Downloaded from https://chemistry-europe.onlinelibrary.wiley.com/doi/10.1002/chem.202401850 by Technische Universitaet Dortmund, Wiley Online Library on [28/07/2026]. See the Terms and Conditions (https://onlinelibrary.wiley.com/terms-and-conditions) on Wiley Online Library for rules of use; OA articles are governed by the applicable Creative Commons License

tetrakis(triphenylphosphine) palladium (54.8 mg, 0.047 mmol, 0.05 equiv.) was added. After stirring the mixture for 15 h at 90 °C and cooling down to room temperature, the product was extracted with dichloromethane (25 mL×3). The organic phase was separated, dried over $MgSO_4$ and filtered. The solvent was removed under reduced pressure. The product mixture was purified via column chromatography on silica gel (CH_2Cl_2/CH_3OH, 1:0–20:1–13:1) and ligand **L1** ($C_{37}H_{31}N_3O$, 533.68 g/mol, 316 mg, 0.592 mmol, 63 %) was obtained as a bright yellow crystalline solid.

^{1}H NMR (700 MHz, DMSO, aromatic region) δ 9.28 (s, 1H), 8.60 (s, 1H), 8.53–8.50 (m, 1H), 8.14–8.09 (m, 2H), 8.06 (dd, *J* = 8.3, 1.1 Hz, 1H), 7.98 (d, *J* = 5.5 Hz, 1H), 7.91 (dd, *J* = 8.3, 7.0 Hz, 1H), 7.74 (dd, *J* = 7.1, 1.1 Hz, 1H). **^{13}C NMR** (176 MHz, DMSO) δ 176.89, 150.30, 143.39, 141.58, 139.28, 136.39, 136.35, 131.63, 130.89, 129.23, 128.15, 126.96, 122.19, 117.29, 79.65, 46.21, 40.50, 40.39, 40.37, 40.27, 40.25, 40.13, 40.01, 39.89, 39.77, 39.65, 31.58, 27.55, 26.25, 22.69, 14.42 **HR ESI-MS** (*m/z*): measured for **L1** + H: 534.2507; calculated: 534.2540.

Synthesis of Helicate H [Pd_2(L1)$_4$]

450 μL of a 3.11 mM solution of **L1** in CD_3CN and 50 μL of a 15 mM solution of $[Pd(CH_3CN)_4](BF_4)_2$ in CD_3CN were mixed in an NMR tube and shaken vigorously. The mixture was then heated to 70 °C for 24 h to afford helicate $[Pd_2(\mathbf{L1})_4]$ (**H**).

^{1}H NMR (600 MHz, CD_3CN, aromatic region) δ 8.82 (s, 1H), 8.65 (s, 1H), 7.82 (t, *J* = 7.9 Hz, 1H), 7.76 (d, *J* = 6.4 Hz, 1H), 7.73 (d, *J* = 8.4 Hz, 1H), 7.48 (d, *J* = 6.4 Hz, 1H), 7.32 (d, *J* = 2.4 Hz, 1H), 7.25 (d, *J* = 7.6 Hz, 2H). **^{13}C NMR** (151 MHz, CD_3CN) δ 177.63, 155.39, 143.86, 141.16, 139.62, 137.42, 135.89, 134.63, 130.60, 129.10, 128.66, 126.81, 126.09, 124.79, 121.25, 117.90, 116.95, 46.29, 31.78, 27.94, 26.52, 23.03, 13.94, 1.32, 1.18, 1.04, 0.90, 0.77, 0.63, 0.49. **HR ESI-MS** (*m/z*): measured for $[Pd_2(\mathbf{L1})_4]^{4+}$: 586.7002; calculated: 586.6894.

Synthesis of Mesocate M [Pd_2(L1)$_4$]

450 μL of a 3.11 mM solution of **L1** in DMSO-d_6 and 50 μL of a 15 mM solution of $[Pd(CH_3CN)_4](OTf)_2$ in DMSO-d_6 were mixed in an NMR tube and shaken vigorously. The mixture was then heated to 70 °C for 24 h to afford mesocate $[Pd_2(\mathbf{L1})_4]$ (**M**).

^{1}H NMR (600 MHz, DMSO, aromatic region) δ 9.56 (d, *J* = 6.6 Hz, 1H), 9.48 (s, 1H), 9.30 (s, 1H), 9.01 (d, *J* = 6.7 Hz, 1H), 8.79 (d, *J* = 2.1 Hz, 1H), 8.68 (d, *J* = 2.3 Hz, 1H), 8.39 (d, *J* = 6.6 Hz, 1H), 8.37 (d, *J* = 6.7 Hz, 1H), 8.23 (d, *J* = 8.2 Hz, 1H), 8.17–8.13 (m, 2H), 8.06 (d, *J* = 7.4 Hz, 1H), 8.05–8.02 (m, 1H), 7.80 (d, *J* = 6.8 Hz, 1H), 7.32–7.22 (m, 2H), 6.79 (d, *J* = 9.5 Hz, 1H), 6.66 (d, *J* = 8.6 Hz, 1H). **HR ESI-MS** (*m/z*): measured for $[Pd_2(\mathbf{L1})_4]^{4+}$: 586.7005; calculated: 586.6894.

Synhesis of Heteroleptic Cage [Pd_2(L1)$_2$(L2)$_2$]

225 μL of 3.11 mM solutions of **L1** and **L2** in CD_3CN and 50 μL of a 15 mM solution of $[Pd(CH_3CN)_4](BF_4)_2$ in CD_3CN were mixed in an NMR tube and shaken vigorously. The mixture was then heated to 70 °C for 24 h to afford heteroleptic cage $[Pd_2(\mathbf{L1})_2(\mathbf{L2})_2]$.

^{1}H NMR (600 MHz, CD_3CN, aromatic region) δ 9.71 (s, 1H), 9.57 (s, 1H), 9.27 (d, *J* = 6.7 Hz, 1H), 8.99 (dd, *J* = 5.8, 1.2 Hz, 1H), 8.65 (d, *J* = 2.3 Hz, 1H), 8.44 (ddd, *J* = 8.4, 2.0, 1.0 Hz, 1H), 8.21 (d, *J* = 6.7 Hz, 1H), 8.07–8.01 (m, 2H), 7.94–7.85 (m, 3H), 7.67 (dd, *J* = 7.9, 5.8 Hz, 1H), 7.51 (dd, *J* = 6.9, 1.0 Hz, 1H), 7.13 (dd, *J* = 8.7, 2.3 Hz, 1H), 6.91 (d, *J* = 8.8 Hz, 1H). **^{13}C NMR** (151 MHz, CD_3CN) δ 189.62, 178.19, 154.08, 151.55, 147.37, 144.85, 141.94, 141.84, 140.94, 138.10, 137.50, 137.37, 135.73, 135.68, 135.39, 134.32, 133.70, 133.09, 132.42, 128.22, 128.16, 128.12, 127.03, 125.57, 123.94, 123.55, 122.26, 117.91, 117.02, 44.41, 31.23, 29.96, 26.42, 26.07, 22.69, 13.76, 1.48, 1.31, 1.17, 1.04, 0.90, 0.76, 0.62, 0.49. **HR ESI-MS** (*m/z*): measured for $[Pd_2(\mathbf{L1})_2(\mathbf{L2})_2]^{4+}$: 487.1288; calculated: 487.1311.

Supporting Information Summary

The authors have cited additional references within the Supporting Information.[48–59]

Acknowledgements

This work was supported by the Deutsche Forschungsgemeinschaft (DFG) trough GRK2376 ("Confinement-Controlled Chemistry", project number 331085229). Funded by the Deutsche Forschungsgemeinschaft (DFG, German Research Foundation) under Germany's Excellence Strategy – EXC 2033-390677874 – RESOLV. Diffraction data of $[Pd_2\mathbf{L1}_4]$, $[Pd_6\mathbf{L1}_{12}]$ and $[Pd_2\mathbf{L1}_2\mathbf{L2(b)}_2]$ was collected at PETRA III and processed on the Maxwell computational resources operated at DESY (Hamburg, Germany) a member of the Helmholtz Association (HGF).[60] We thank Guillaume Pompidor and Eva Crosas for assistance at synchrotron beamline P11 (I-20210921) and DESY user office for travel funds. Open Access funding enabled and organized by Projekt DEAL.

Conflict of Interests

The authors declare no conflict of interest.

Data Availability Statement

The data that support the findings of this study are available from the corresponding author upon reasonable request.

Keywords: Self-assembly · Cages · Heteroleptic assembly · Stimuli response · Systems chemistry

[1] R. Nussinov, *Chem. Rev.* **2016**, *116*, 6263–6266.
[2] S. Raman, *Biochemistry-us* **2018**, *57*, 376–382.
[3] S. A. Coulocheri, D. G. Pigis, K. A. Papavassiliou, A. G. Papavassiliou, *Biochimie* **2007**, *89*, 1291–1303.
[4] U. S. Bhalla, R. Iyengar, *Science* **1999**, *283*, 381–387.
[5] S. Pullen, J. Tessarolo, G. H. Clever, *Chem. Sci.* **2021**, *12*, 7269–7293.
[6] E. Benchimol, I. Regeni, B. Zhang, M. Kabiri, J. J. Holstein, G. H. Clever, *J. Am. Chem. Soc.* **2024**, *146*, 6905–6911.
[7] E. G. Percástegui, *Eur. J. Inorg. Chem.* **2021**, *2021*, 4425–4438.
[8] E. Benchimol, B.-N. T. Nguyen, T. K. Ronson, J. R. Nitschke, *Chem. Soc. Rev.* **2022**, *51*, 5101–5135.
[9] S. J. Wezenberg, *Chem. Lett.* **2020**, *49*, 609–615.
[10] D. A. Roberts, B. S. Pilgrim, J. R. Nitschke, *Chem. Soc. Rev.* **2017**, *47*, 626–644.
[11] V. Croué, S. Goeb, M. Sallé, *Chem. Commun.* **2015**, *51*, 7275–7289.
[12] E. Benchimol, J. Tessarolo, G. H. Clever, *Nat. Chem.* **2024**, *16*, 13–21.
[13] S. Wang, T. Sawada, M. Fujita, *Chem. Commun.* **2016**, *52*, 11653–11656.

© 2024 The Authors. Chemistry - A European Journal published by Wiley-VCH GmbH

15213765, 2024, 46, Downloaded from https://chemistry-europe.onlinelibrary.wiley.com/doi/10.1002/chem.202401850 by Technische Universitaet Dortmund, Wiley Online Library on [28/07/2026]. See the Terms and Conditions (https://onlinelibrary.wiley.com/terms-and-conditions) on Wiley Online Library for rules of use; OA articles are governed by the applicable Creative Commons License

[14] P. Cheng, L. Cai, S. Li, S. Hu, D. Yan, L. Zhou, Q. Sun, *Angew. Chem. Int. Ed.* **2020**, *59*, 23569–23573.
[15] D. Zhang, Q. Gan, A. J. Plajer, R. Lavendomme, T. K. Ronson, Z. Lu, J. D. Jensen, B. W. Laursen, J. R. Nitschke, *J. Am. Chem. Soc.* **2022**, *144*, 1106–1112.
[16] V. Croué, S. Goeb, G. Szalóki, M. Allain, M. Sallé, *Angew. Chem. Int. Ed.* **2015**, *55*, 1746–1750.
[17] W. Cullen, S. Turega, C. A. Hunter, M. D. Ward, *Chem. Sci.* **2014**, *6*, 625–631.
[18] H. Lee, J. Tessarolo, D. Langbehn, A. Baksi, R. Herges, G. H. Clever, *J. Am. Chem. Soc.* **2022**, *7*, 3099–3105.
[19] A. Ghosh, J. Pruchyathamkorn, C. F. Espinosa, J. R. Nitschke, *J. Am. Chem. Soc.* **2024**, *146*, 2568–2573.
[20] Y. Yang, T. K. Ronson, J. Zheng, N. Mihara, J. R. Nitschke, *Chem* **2023**, *9*, 1972–1982.
[21] Y. Gu, E. A. Alt, H. Wang, X. Li, A. P. Willard, J. A. Johnson, *Nature* **2018**, *560*, 65–69.
[22] J. Zhao, E. O. Bobylev, D. J. Lundberg, N. J. Oldenhuis, H. Wang, I. Kevlishvili, S. L. Craig, H. J. Kulik, X. Li, J. A. Johnson, *J. Am. Chem. Soc.* **2023**, *145*, 21879–21885.
[23] R.-J. Li, J. Tessarolo, H. Lee, G. H. Clever, *J. Am. Chem. Soc.* **2021**, *143*, 3865–3873.
[24] L.-X. Cai, D.-N. Yan, P.-M. Cheng, J.-J. Xuan, S.-C. Li, L.-P. Zhou, C.-B. Tian, Q.-F. Sun, *J. Am. Chem. Soc.* **2021**, *143*, 2016–2024.
[25] K. Endo, H. Ube, M. Shionoya, *J. Am. Chem. Soc.* **2019**, *142*, 407–416.
[26] A. E. M. Díaz, J. E. M. Lewis, *Front. Chem.* **2021**, *9*, 706462.
[27] D. Zhang, T. K. Ronson, L. Xu, J. R. Nitschke, *J. Am. Chem. Soc.* **2020**, *142*, 9152–9157.
[28] K. Matsumoto, S. Kusaba, Y. Tanaka, Y. Sei, M. Akita, K. Aritani, M. Haga, M. Yoshizawa, *Angew. Chem. Int. Ed.* **2019**, *58*, 8463–8467.
[29] D.-N. Yan, L.-X. Cai, P.-M. Cheng, S.-J. Hu, L.-P. Zhou, Q.-F. Sun, *J. Am. Chem. Soc.* **2021**, *143*, 16087–16094.
[30] L.-J. Wang, X. Li, S. Bai, Y.-Y. Wang, Y.-F. Han, *J. Am. Chem. Soc.* **2020**, *142*, 2524–2531.
[31] W. M. Bloch, J. J. Holstein, W. Hiller, G. H. Clever, *Angew. Chem. Int. Ed.* **2017**, *56*, 8285–8289.
[32] S. Sudan, F. Fadaei-Tirani, R. Scopelliti, K. E. Ebbert, G. H. Clever, K. Severin, *Angew. Chem. Int. Ed.* **2022**, *61*, e202201823.
[33] W. M. Bloch, Y. Abe, J. J. Holstein, C. M. Wandtke, B. Dittrich, G. H. Clever, *J. Am. Chem. Soc.* **2016**, *138*,13750–13755.
[34] S. Sudan, F. Fadaei-Tirani, K. Severin, *Chem. Commun.* **2023**, *59*, 8258–8261.
[35] W. M. Bloch, S. Horiuchi, J. J. Holstein, C. Drechsler, A. Wuttke, W. Hiller, R. A. Mata, G. H. Clever, *Chem. Sci.* **2023**, *14*, 1524–1531.
[36] M. Bhol, R. L. Borkar, B. Shankar, S. K. Panda, M. Wolff, M. Sathiyendiran, *Inorg. Chem.* **2023**, *62*, 11554–11569.
[37] E. Chinnaraja, R. Arunachalam, E. Suresh, S. K. Sen, R. Natarajan, P. S. Subramanian, *Inorg. Chem.* **2019**, *58*, 4465–4479.
[38] A. P. Paneerselvam, S. S. Mishra, D. K. Chand, *J. Chem. Sci.* **2018**, *130*, 96.
[39] F. Cui, S. Li, C. Jia, J. S. Mathieson, L. Cronin, X.-J. Yang, B. Wu, *Inorg. Chem.* **2012**, *51*, 179–187.
[40] S. Carlotto, L. Armelao, M. Rancan, *Int. J. Mol. Sci.* **2022**, *23*, 10619.
[41] T. Zhang, L.-P. Zhou, X.-Q. Guo, L.-X. Cai, Q.-F. Sun, *Nat. Commun.* **2017**, *8*, 15898.
[42] M. Käseborn, J. J. Holstein, G. H. Clever, A. Lützen, *Angew. Chem. Int. Ed.* **2018**, *57*, 12171–12175.
[43] L. Neukirch, M. D. Kulas, J. J. Holstein, G. H. Clever, *Chem. Eur. J.* **2024**, *30*, e202400132.
[44] S. Maki-Yonekura, R. Matsuoka, Y. Yamashita, H. Shimizu, M. Tanaka, F. Iwabuki, K. Yonekura, *eLife* **2018**, *7*, e35419.
[45] W. Chen, J. Dev, J. Mezhyrova, L. Pan, A. Piai, J. J. Chou, *Structure* **2018**, *26*, 627–634.e4.
[46] A. Stephenson, S. P. Argent, T. Riis-Johannessen, I. S. Tidmarsh, M. D. Ward, *J. Am. Chem. Soc.* **2011**, *133*, 858–870.
[47] A. W. Markwell-Heys, M. L. Schneider, J. M. L. Madridejos, G. F. Metha, W. M. Bloch, *Chem. Commun.* **2021**, *57*, 2915–2918.
[48] J. Tessarolo, H. Lee, E. Sakuda, K. Umakoshi, G. H. Clever, *J. Am. Chem. Soc.* **2021**, *143*, 6339–6344.
[49] K. E. Ebbert, L. Schneider, A. Platzek, C. Drechsler, B. Chen, R. Rudolf, G. H. Clever, *Dalton Trans.* **2019**, *48*, 11070–11075.
[50] A. Burkhardt, T. Pakendorf, B. Reime, J. Meyer, P. Fischer, N. Stübe, S. Panneerselvam, O. Lorbeer, K. Stachnik, M. Warmer, P. Rödig, D. Göries, A. Meents, *Eur. Phys. J. Plus* **2016**, *131*, 56.
[51] W. Kabsch, *Acta Crystallogr. Sect. D: Biological Crystallogr.* **2010**, *66*, 125–132.
[52] G. M. Sheldrick, *Acta Crystallogr. Sect. A: Found Crystallogr.* **2008**, *64*, 112–122.
[53] G. M. Sheldrick, *Acta Crystallogr. Sect. C: Struct. Chem.* **2015**, *71*, 3–8.
[54] C. B. Hübschle, G. M. Sheldrick, B. Dittrich, *J. Appl. Crystallogr.* **2011**, *44*, 1281–1284.
[55] D. Kratzert, J. J. Holstein, I. Krossing, *J. Appl. Crystallogr.* **2015**, *48*, 933–938.
[56] D. Kratzert, I. Krossing, *J. Appl. Crystallogr.* **2018**, *51*, 928–934.
[57] A. Thorn, B. Dittrich, G. M. Sheldrick, *Acta Crystallogr. Sect. A: Found Crystallogr.* **2012**, *68*, 448–451.
[58] A. L. Spek, *Acta Crystallogr. Sect. C: Struct. Chem.* **2015**, *71*, 9–18.
[59] A. L. Spek, *Acta Crystallogr. Sect. D: Biological Crystallogr.* **2009**, *65*, 148–155.
[60] Deposition Numbers "2328293 (for [Pd_6**L1**$_{12}$]), 2328294 (for [Pd_2**L1**$_2$**L2b**$_2$]) and 2328295 (for [Pd_2**L1**$_4$])" contain the supplementary crystallographic data for this paper. These data are provided free of charge by the joint Cambridge Crystallographic Data Centre and Fachinformationszentrum Karlsruhe "Access Structures service".

Manuscript received: May 26, 2024
Accepted manuscript online: June 10, 2024
Version of record online: July 26, 2024

© 2024 The Authors. Chemistry - A European Journal published by Wiley-VCH GmbH

15213765, 2024, 46, Downloaded from https://chemistry-europe.onlinelibrary.wiley.com/doi/10.1002/chem.202401850 by Technische Universitaet Dortmund, Wiley Online Library on [28/07/2026]. See the Terms and Conditions (https://onlinelibrary.wiley.com/terms-and-conditions) on Wiley Online Library for rules of use; OA articles are governed by the applicable Creative Commons License